

This is the peer reviewed version of the following article:

Dynamically feasible motions of a class of purely-translational cable-suspended parallel robots / Mottola, G., Gosselin, C., Carricato, M.. - In: MECHANISM AND MACHINE THEORY. - ISSN 0094-114X. - 132:(2019), pp. 193-206. [10.1016/j.mechmachtheory.2018.10.017]

Terms of use:

The terms and conditions for the reuse of this version of the manuscript are specified in the publishing policy. For all terms of use and more information see the publisher's website.

04/06/2026 02:13

(Article begins on next page)

This is the final peer-reviewed accepted manuscript of:

Giovanni Mottola, Clément Gosselin, Marco Carricato, *Dynamically feasible motions of a class of purely-translational cable-suspended parallel robots*, Mechanism and Machine Theory, Volume 132, 2019, Pages 193-206

ISSN 0094-114X

The final published version is available online at:

<https://doi.org/10.1016/j.mechmachtheory.2018.10.017>

© 2018. This manuscript version is made available under the Creative Commons Attribution-NonCommercial-NoDerivs (CC BY-NC-ND) 4.0 International License (<http://creativecommons.org/licenses/by-nc-nd/4.0/>)

Highlights

- A cable-suspended robot is presented with a spatial purely translational motion.
- Several special architectures are identified with distinctive and useful features.
- The singularity-free/reachable/interference-free workspaces are analytically found.
- The theoretical findings are validated by experimental tests.
- The robot can perform dynamic trajectories outside the static equilibrium workspace.

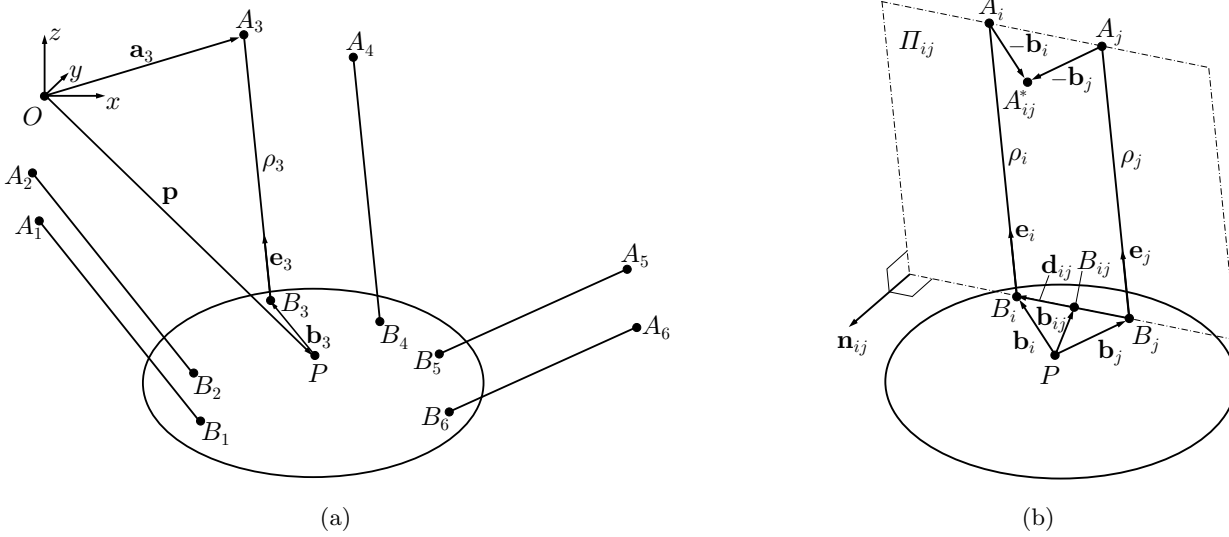


Figure 1: Left: a 6-cable CSPPR with three translational DOFs. Right: The planar parallelogram formed by cables i and j .

Since the EE preserves its orientation throughout any non-singular motion, all vectors fixed to the EE, such as \mathbf{b}_i ($i = 1, \dots, 6$), are constant.

3. Kinetostatic model

The forces exerted by the parallel cables i and j on the EE are $\mathbf{F}_i = \tau_i \mathbf{e}_i$ and $\mathbf{F}_j = \tau_j \mathbf{e}_j = \tau_j \mathbf{e}_i$. The resultant force and the resultant moment about P are, respectively (Fig. 1b)

$$\mathbf{F}_{tot,ij} = \mathbf{F}_i + \mathbf{F}_j = \mathbf{e}_i(\tau_i + \tau_j) \quad (1a)$$

$$\mathbf{M}_{tot,ij} = \mathbf{b}_i \times \mathbf{F}_i + \mathbf{b}_j \times \mathbf{F}_j = (\tau_i \mathbf{b}_i + \tau_j \mathbf{b}_j) \times \mathbf{e}_i \quad (1b)$$

It can be easily shown that this system of two forces is equivalent to a single force $\mathbf{F}_{ij} = \mathbf{e}_i \tau_{tot,ij}$ applied in point B_{ij} whose position is given by $\mathbf{p} + \mathbf{b}_{ij}$, where $\tau_{tot,ij} = \tau_i + \tau_j$, and

$$\mathbf{b}_{ij} = \frac{\tau_i \mathbf{b}_i + \tau_j \mathbf{b}_j}{\tau_{tot,ij}} = \sigma_i \mathbf{b}_i + \sigma_j \mathbf{b}_j = \sigma_i \mathbf{b}_i + (1 - \sigma_i) \mathbf{b}_j \quad (2)$$

where σ_i, σ_j are the tension ratios² defined as

$$\sigma_i = \frac{\tau_i}{\tau_{tot,ij}}, \quad \sigma_j = \frac{\tau_j}{\tau_{tot,ij}} = 1 - \sigma_i \quad (3)$$

By definition (2), B_{ij} lies on the line passing through B_i and B_j . B_{ij} coincides with one of the endpoints if either $\sigma_i = 0$ or $\sigma_i = 1$; from Eq. (3), this is equivalent to $\tau_i = 0$ or $\tau_j = 0$, respectively. If both cables are taut, then $0 \leq \tau_i, \tau_j \leq \tau_{tot,ij}$, so $0 \leq \sigma_i, \sigma_j \leq 1$ and, consequently, B_{ij} lies on the segment $\overline{B_i B_j}$.

If m is the EE mass, $\mathbf{g} = [0, 0, -g]^T$ is the gravitational acceleration, and no wrenches other than gravity and inertia act on the platform, the dynamic equilibrium of the robot yields

$$\sum_{i=1}^6 \mathbf{e}_i \tau_i = m \ddot{\mathbf{p}} - m \mathbf{g} = -\mathbf{F}_e \quad (4a)$$

$$\sum_{i=1}^6 \mathbf{b}_i \times \mathbf{e}_i \tau_i = \mathbf{0} \quad (4b)$$

where the sum of gravity and inertial effects, $\mathbf{F}_e = m(\mathbf{g} - \ddot{\mathbf{p}})$, does not contribute to the moment equilibrium around P . We thus have a linear system of six equations in six unknowns, i.e. the cable tensions τ_1, \dots, τ_6 . This system can be simplified

²The definitions in Eqs. (2) and (3) are not valid if $\tau_{tot,ij} = 0$; however, this means either that one of the tensions is negative (against the assumption of cables being taut) or that $\tau_i = \tau_j = 0$. In this case, the parallelogram is not constraining the rotation along direction \mathbf{n}_{ij} , and the robot can no longer be considered translational.

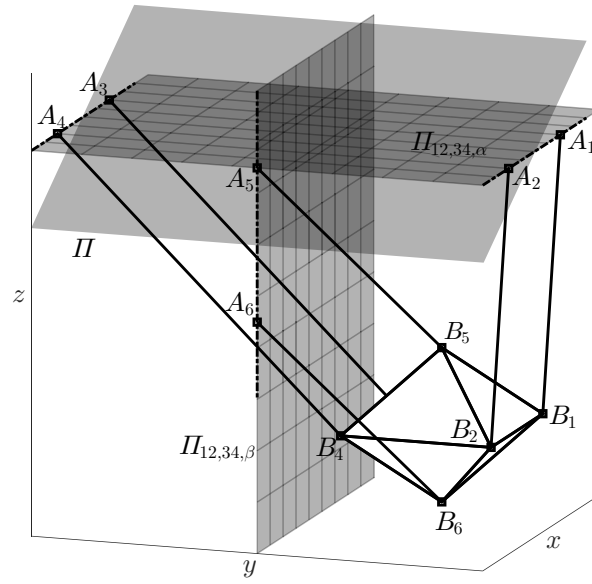


Figure 4: A simplified architecture, with the spools of cables 1 – 2 and 3 – 4 having parallel axes. The rotational singularity planes $\Pi_{ij,kl,\alpha}$ and $\Pi_{ij,kl,\beta}$ are shown with grid lines; the translational singularity plane Π is shown with no grid.

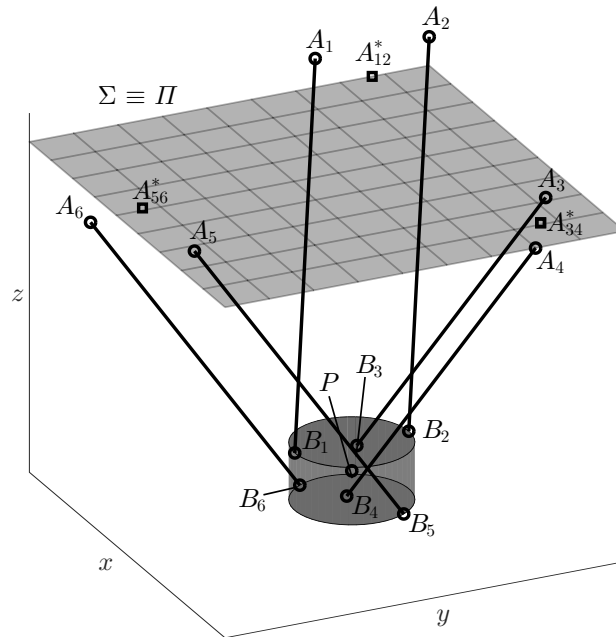


Figure 5: A simplified architecture with lines A_1A_2 , A_3A_4 and A_5A_6 parallel to the plane Π through A_{12}^* , A_{34}^* and A_{56}^* .

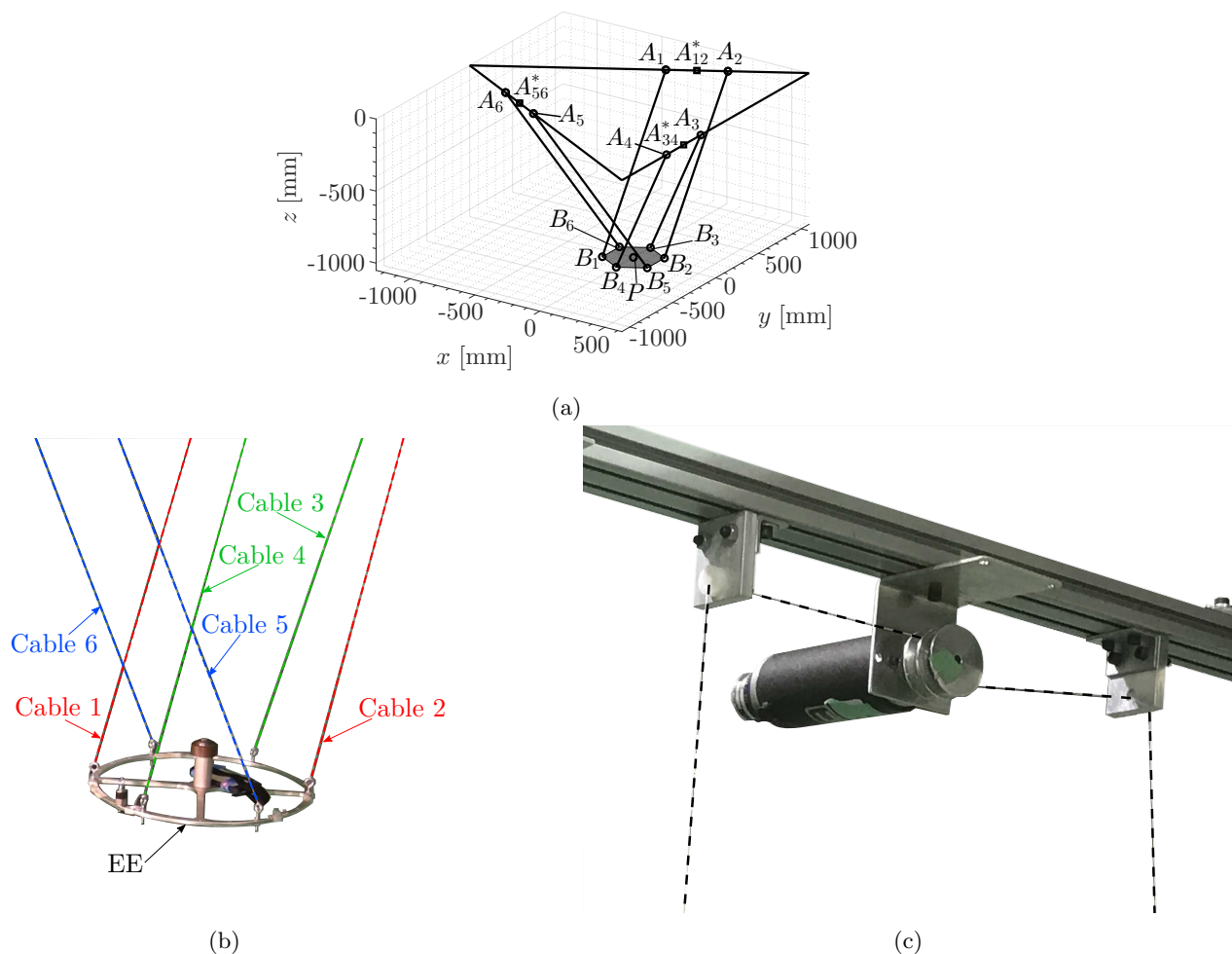


Figure 7: (a): a schematic of the prototype in the reference pose. The fixed frame $Oxyz$ has its origin in the plane of points A_i 's, in the centre of the SEW. (b): top view of the prototype developed at Université Laval. (c): a photo of one of the robot winches, with two cables (highlighted by dashed lines) coiling on the same pulley.

The results can be seen in the attached video, showing the robot as it performs dynamic trajectories such as those presented in [5, 9]; the video shows the robot from two different viewpoints, one frontal and another above the robot. The robot is clearly moving outside the SEW (marked by a grey volume in the video) while keeping positive cable tensions and maintaining a constant orientation; also, it is easy to see that the cables remain parallel as the robot moves.

The video is divided in two parts:

- First, the robot performs a dynamic periodic trajectory such as those presented in [9]: the robot starts from rest and oscillates with increasing motion amplitudes until it moves along a horizontal circle centred in the centre of the SEW and having a radius larger than the workspace. After a few cycles, the robot is slowed down to its starting point (see Fig. 8a for a 3D plot of the trajectory).
- In the second part, we perform point-to-point dynamic motions reaching outside the SEW. At the target points the robot velocity is zero, but not the acceleration (the robot cannot be at rest out of the SEW); here, we used the method in [5] to plan the trajectories (see Fig. 8b).

The robot used for the tests is a prototype meant to be a proof of concept, thus not fully engineered. In any case, we verified that the desired trajectories were followed with an acceptable degree of accuracy, given the limitations of the prototype. We compared the desired position \mathbf{p}_d along the motion with the estimated actual one \mathbf{p}_e : this is obtained by solving the forward kinematics with the real cable lengths $\rho_{i,e}$ as inputs (measured by the encoders on the robot motors). The plots of the norm of the difference $d\mathbf{p} = \mathbf{p}_e - \mathbf{p}_d$ between the desired and the actual periodic and point-to-point trajectories are shown in Figs. 8c and 8d, respectively. We found that the maximum positioning error during the periodic

⁵In this case, the two cables are either always crossing or never crossing, for any position of the robot.

⁶ P does not have to be in the plane through points B_i 's; if it is so, then $\Pi \equiv \Gamma$.

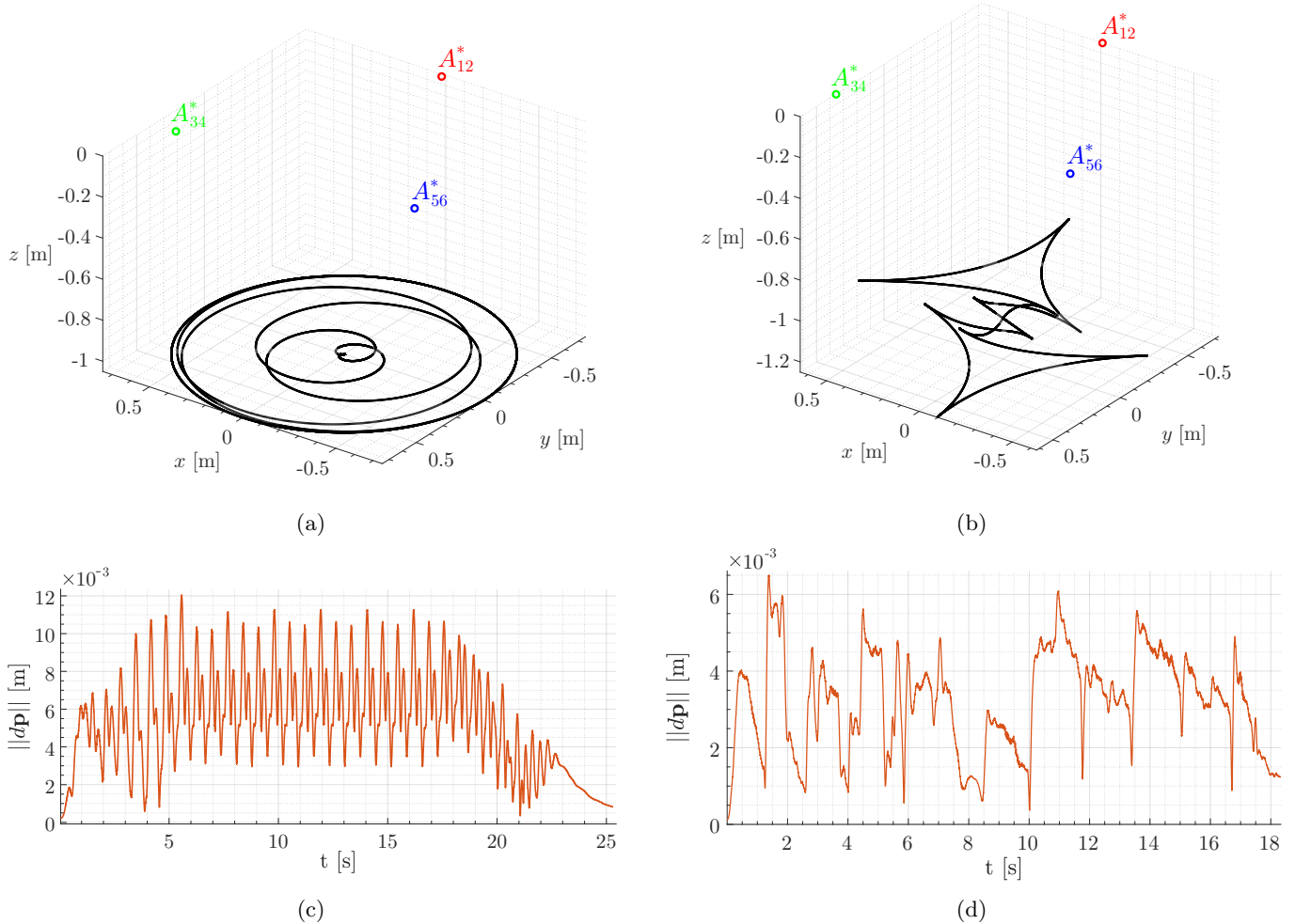


Figure 8: (a): 3D plot of the periodic motion. (b): 3D plot of the point-to-point motion. (c): plot of the position error $\|d\mathbf{p}\|$ along the periodic motion ($d\mathbf{p}$ is the distance between desired position \mathbf{p}_d and the actual one \mathbf{p}_e). (d): plot of $\|d\mathbf{p}\|$ along the point-to-point motion.

motion was 1.205×10^{-2} m, with an average error of 5.36×10^{-3} m (respectively, 6.5×10^{-3} m and 3.2×10^{-3} m for the point-to-point motion). Considering the limitations of the prototype and that the robot was moving with high accelerations (up to $\sim 6.6 \text{ m/s}^2$ during our tests) in a workspace that is meters wide, these errors can be considered to be acceptable.

To verify that the orientation was constant as the robot moved, we recorded the roll, pitch and yaw angles of the platform during the experiments by using the Inertial Measurement Unit (IMU) in a common smartphone that was secured on the robot platform. An example of the results can be seen in Fig. 9: the platform never rotated by more than 3° with respect its start pose, which seems an acceptable error given the approximations in the measurement of the architecture parameters. Such results are compatible with what was observed in [21], where the authors performed a multibody simulation of the dynamic behavior of a CSPR with a cable architecture similar to the one proposed here (except that the robot only moved in a vertical plane and employed eight cables, thus being overconstrained), observing a variation of the EE Euler angles not bigger than 1° . Given that in our case the accelerations are an order of magnitude higher and the robot moves outside its SEW, a larger orientation error is to be expected, also considering the very simple mechanical realization of the tested prototype.⁷

A potential issue of the special architecture defined in Sec. 4 is that it requires a careful design of the EE to ensure that its center of mass (CoM) is sufficiently close to the position of P , as an error in the estimation of the CoM location can produce an orientation error on the EE. Indeed, during some of our tests we did experience small orientation errors when the CoM was displaced from its nominal position in P ; in any case, in the experiments presented in this paper the location of the CoM was accurately chosen in order to respect the condition in Sec. 4.

⁷Since a smartphone IMU is not a precision instrument (the RMS error on the orientation angles in dynamic conditions can be up to roughly 2° [49]), the results reported in Fig. 9 must not be intended as an accurate quantitative assessment of the orientation error. However, they provide a clear indication that the EE orientation remains reasonably constant.

- [47] S. Perreault, P. Cardou, C. Gosselin, M. Otis, Geometric determination of the interference-free constant-orientation workspace of parallel cable-driven mechanisms, *ASME J. Mech. Rob.* 2 (3) (2010) 031016. doi:10.1115/1.4001780.
- [48] L. Blanchet, J.-P. Merlet, Interference detection for cable-driven parallel robots (CDPRs), in: 2014 IEEE/ASME Int. Conf. on Advanced Intelligent Mechatronics, Besançon, France, 2014, pp. 1413–1418. doi:10.1109/AIM.2014.6878280.
- [49] Q. Mourcou, A. Fleury, C. Franco, F. Klopčič, N. Vuillerme, Performance evaluation of smartphone inertial sensors measurement for range of motion, *Sensors* 15 (9) (2015) 23168–23187. doi:10.3390/s150923168.